Journal of Medical Imaging

MedicalImaging.SPIEDigitalLibrary.org

Anthropomorphic dual-lattice voxel models for optimizing image quality and dose

Nina Petoussi-Henss
Helmut Schlattl
Janine Becker
Matthias Greiter
Maria Zankl
Christoph Hoeschen

SPIE.

Nina Petoussi-Henss, Helmut Schlattl, Janine Becker, Matthias Greiter, Maria Zankl, Christoph Hoeschen, "Anthropomorphic dual-lattice voxel models for optimizing image quality and dose," *J. Med. Imag.* **4**(1), 013509 (2017), doi: 10.1117/1.JMI.4.1.013509.

Journal of Medical Imaging 4(1), 013509 (Jan–Mar 2017)

Anthropomorphic dual-lattice voxel models for optimizing image quality and dose

Nina Petoussi-Henss,[a,*] Helmut Schlattl,[a] Janine Becker,[a] Matthias Greiter,[b] Maria Zankl,[a] and Christoph Hoeschen[c]
[a]Institute of Radiation Protection, Helmholtz Zentrum München, Neuherberg, Germany
[b]Individual Monitoring Service, Helmholtz Zentrum München, Neuherberg, Germany
[c]Otto-von-Guericke University, Medical Systems, Institute of Medical Technology, Magdeburg, Germany

Abstract. Using numerical simulations, the influence of various imaging parameters on the resulting image can be determined for various imaging technologies. To achieve this, visualization of fine tissue structures needed to evaluate the image quality with different radiation quality and dose is essential. The present work examines a method that employs simulations of the imaging process using Monte Carlo methods and a combination of a standard and higher resolution voxel models. A hybrid model, based on nonlinear uniform rational B-spline and polygon mesh surfaces, was constructed from an existing voxel model of a female patient of a resolution in the range of millimeters. The resolution of the hybrid model was 500 μm, i.e., substantially finer than that of the original model. Furthermore, a high resolution lung voxel model [$(0.11\ \text{mm})^3$ voxel volume, slice thickness: 114 μm] was developed from the specimen of a left lung lobe. This has been inserted into the hybrid model, substituting its left lung lobe and resulting in a dual-lattice geometry model. "Dual lattice" means, in this context, the combination of voxel models with different resolutions. Monte Carlo simulations of radiographic imaging were performed and the fine structure of the lung was easily recognizable. [DOI: 10.1117/1.JMI.4.1.013509]

Keywords: simulation; image; voxel; anthropomorphic; lung; model.

Paper 16247PR received Nov. 16, 2016; accepted for publication Mar. 14, 2017; published online Mar. 30, 2017.

1 Introduction

In radiography, there is generally a conflict between the best image quality and the lowest possible patient dose. A proven method of dosimetry is the simulation of radiation transport in virtual human models (i.e., phantoms). However, while the resolution of these voxel models is adequate for most dosimetric purposes, they cannot provide the required organ fine structures necessary for the assessment of imaging quality. The aim of this work is to develop hybrid/dual-lattice voxel models (called also phantoms) as well as simulation methods by which image quality (and patient dose) for typical radiographic procedures can be determined. By varying image settings and/or patient stature, the relation between dose and image quality would change. The results of this work will provide a basis to investigate, by means of simulations, the relationship between image quality and patient dose for various imaging parameters and develop methods for their optimization.

At present, there exist three different types of computational anthropomorphic models: stylized (or mathematical), voxel (or tomographic), and hybrid types based upon nonlinear uniform rational B-spline (NURBS) and/or polygon mesh (PM) surfaces. The characteristics and advantages of each type of phantom have been reviewed by Bolch et al.[1] Stylized phantoms[2] have been used in radiation dosimetry for over 40 years. They are composed of 3-D geometric surface equations defining both internal organs and outer body surfaces. While they are flexible in terms of allowing changes in organ size, body shape, and extremity positioning, they are generally insufficient with respect to anatomic realism. Voxel phantoms, in contrast, are composed of a three-dimensional array of volume elements (voxels), each with a unique organ identity, elemental composition, and density. Voxel phantoms are assembled through segmentation of individual image slices from computed tomography (CT), magnetic resonance or other image data, thus they provide a high level of anatomic realism.[3–5] Their main limitations are that their construction is time-consuming and their inflexibility of adjustment to match individuals other than the person providing the source data. The third generation of phantoms is the so-called hybrid type; the organs are described by either NURBS or PM surfaces.[6–8] This offers both flexibility in organ alterations and anatomical realism. While most of the hybrid phantoms were applied for dosimetry, Segars et al.[9] generated 58 adult highly detailed 4-D extended cardiac-torso (XCAT) phantoms based on patient CT data to be used for imaging research. Several works are reported attempting computational modelling of the lung.[10] Recently, Becchetti et al.[11] developed a realistic model of the anatomical texture from the pulmonary interstitium aiming to extend the capability of those anthropomorphic computational phantoms, allowing for more accurate image quality assessment. Jimenez-Carretero et al.[12] developed a technique to generate computational anthropomorphic CT phantoms of the human lung automatically from biological and image-based data and created a dataset of 24 labeled anthropomorphic pulmonary CT phantoms. Furthermore, computational phantoms of the breast were developed for multimodality imaging research. Similarly to the phantoms developed

*Address all correspondence to: Nina Petoussi-Henss, E-mail: petoussi@helmholtz-muenchen.de

2329-4302/2017/$25.00 © 2017 SPIE

for dosimetry, the earlier type were the so-called rule-based models of the breast, whose anatomy is defined by mathematical equations. The most sophisticated models of this type are those of Bakic et al.[13–15] To improve anatomical realism, voxelized breast phantoms have been developed from dedicated breast CT data from mastectomy specimens.[16,17] Due to limited access to specimens and because these do not represent whole, intact breasts, realistic computational breast phantoms were created based on human subjects via segmentation of *in vivo* breast CT imaging data.[18–20] These phantoms provide a large population of a wide range of breast types, volumes, and parenchymal patterns.[20]

Since the main purpose of most of the existing whole-body anthropomorphic models is the computation of organ/tissue doses for ionizing radiation or electromagnetic fields, their resolution is generally in the order of a few millimeters. Thus, they are not suited to simulate realistic images for which the desired resolution is of the order of micrometers. Moreover, whole-body high-resolution human models can hardly be obtained due to radiation dose constraints and would be difficult to handle numerically; therefore, dual lattice voxel models, i.e., combined high and lower resolution voxel models, appear to be favorable. Depending on the diagnostic purpose, high-resolution models of certain organs could be incorporated into these patient models. In order to verify that this method is applicable, Monte Carlo simulations of thorax radiography were performed, using a high-resolution lung model embedded in a lower resolution model of the rest of the body. First results have been reported by Petoussi-Henss et al.[21]

2 Methods

2.1 *Whole Body Voxel Model Laura and its NURBS/PM Version*

For this work, the whole body voxel model "Laura,"[3] of an adult female, previously developed at Helmholtz Zentrum München, has been employed. Laura was constructed from CT image data of a 43-year-old female patient. With a 1.68-m height and 59-kg weight, the patient was close to the so-called reference female (1.63 and 60 kg).[22] The voxel in-plane resolution was 1.875 mm and the slice thickness 5 mm, corresponding to a voxel volume of 17.6 mm^3 and ca. 2.6 million of voxels. A total of 88 tissues were primarily segmented in Laura. Figure 1 shows three-dimensional representations of some of the organs of this model. More details about this phantom can be found at Zankl.[3]

As the first results of the simulated images have shown (see Sec. 3.3), the original resolution of Laura was not sufficient to develop simulation methods by which image quality for typical radiographic procedures can be determined, so that part of the model had to be transformed to a NURBS/PM–based hybrid model. The method of constructing NURBS-based models was described, among others, by Lee et al.[7] For the present work, the procedure of this transformation commences with the polygonization of the initial voxel model by separately rendering each organ to a PM surface, using the software IDL 8.2 (Ref. 23). The rendering process resulted in jagged-looking objects, as seen in Fig. 2(a), which had to be smoothed. This is due to the limited resolution on the z-axis, corresponding to the image slice thickness. The PM data were, therefore, exported to the 3-D modeling software, Rhinoceros (version 4.0) (Robert McNeel and Associates, United States). Subsequently, NURBS smooth surfaces were created for each organ. Figure 2 graphically describes an example of the procedure by showing the development of the liver from rendered images of the original voxel model of the (a) liver, (b) the corresponding PM, (c) its NURBS surface model, and finally, (d) the PM model created from the NURBS surfaces.

An exception of this procedure was the skeleton for which polygonization and smoothing could not be performed in an optimal way. This is because the resolution, particularly on the z-axis, was limited, therefore, a good PMs for the skeleton could not be generated. Therefore, the skeleton used for this work was obtained as a PM surface from Ref. 24. The contours of this skeleton were smooth, thus it was not necessary to convert the PM to NURBS but its size and form had to be adjusted to fit the anatomy of the female model Laura. Figure 3 shows part of the original skeleton of the upper torso (rib cage, spine, sternum, scapulae, and clavicles) of the model (a) Laura and (b) the respective parts of the new imported and adjusted skeleton. It can be seen that the original skeleton has nonsmooth surfaces, in contrast to the one which has been implemented. Furthermore, the adopted skeleton includes, besides bone, the cartilage as well, whereas in the original voxel model Laura, cartilage could be only segmented for the lower ribs.

Since the aim of this work was to examine the feasibility of simulation of a radiograph focusing on fine lung structures using

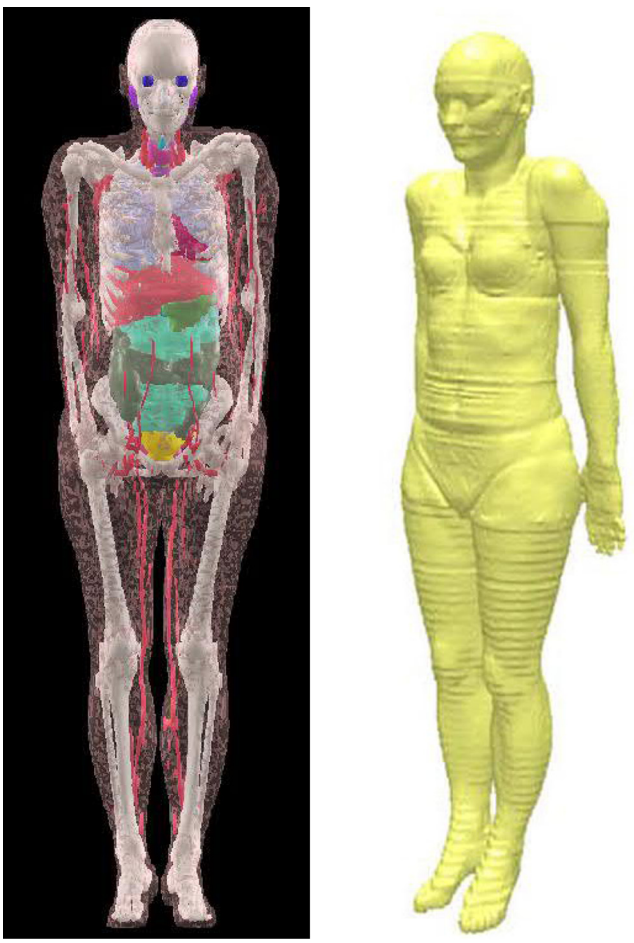

Fig. 1 The whole-body voxel model Laura: (a) 3-D reconstructions of several organs and tissues (for example, lungs, liver, stomach, colon, skeleton, heart, bladder, main blood vessels, etc.) and (b) 3-D reconstruction of skin.

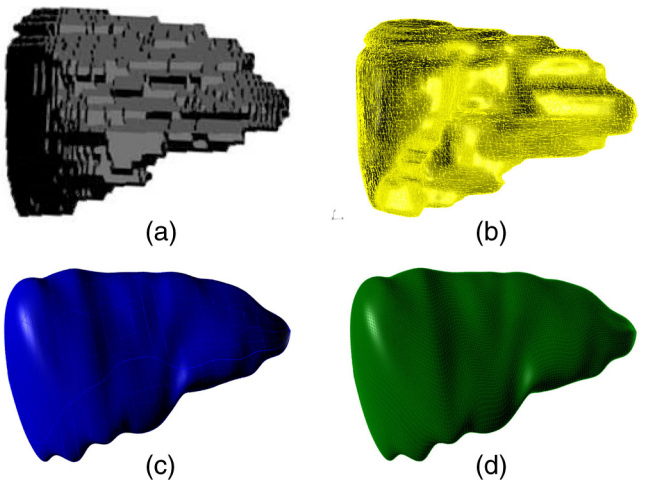

Fig. 2 Rendered images of the liver as an example of the process: original voxel model of the (a) liver, (b) corresponding PM, (c) its NURBS surface model, and (d) PM model from NURBS.

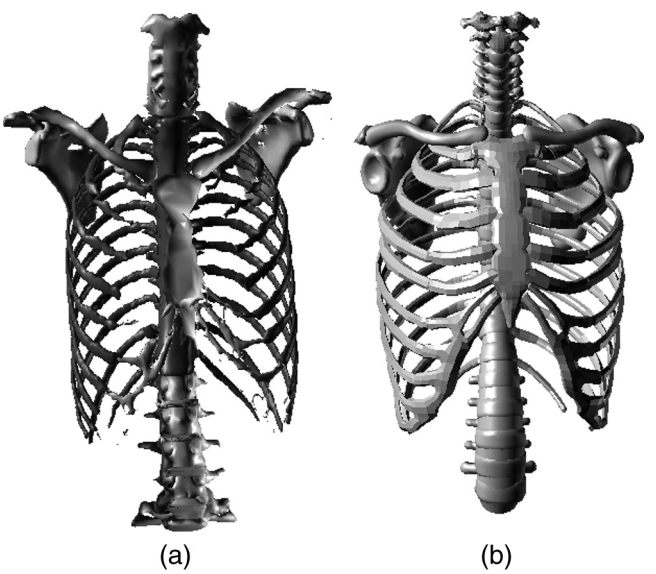

Fig. 3 (a) Parts of the skeleton of the original model Laura. (b) PM skeleton from creativecrash.com used as a substitute of the original skeleton and adjusted to fit the size of the phantom. Cartilage is also shown on picture (b) whereas for the original skeleton (a), cartilage was only partially segmented.

the high-resolution lung model, details in other organs like the blood in the heart and lungs were not accounted for in the NURBS/PM model, as well as air in the lungs. Moreover, bronchi, oesophagus, blood vessels, and muscles were not included.

To date, Monte Carlo radiation transport codes cannot be coupled to NURBS surface geometries, whereas PM geometries could be directly implemented into some Monte Carlo codes. A version of Geant4 is available for direct implementation of PM phantoms, resulting, however, in high computation times.[8] To improve computation speed, Yeom et al.[25] converted PM phantoms to a tetrahedral mesh format via tetrahedralization for use in the Monte Carlo code GEANT4. Moreover, PenMesh, a Monte Carlo code based on PENELOPE physics subroutines, can directly deal with PM geometries.[26] For the present work, the resulting NURBS and PM organs have been revoxelized by triangulation with Rhinoceros and then by voxelization with the software Binvox (Ref. 27). The procedure of model transformation from voxel to NURBS/PM and then back to voxel form has the advantage that a resolution can be assigned to the resulting hybrid voxel model, which is substantially finer than the original one. To keep the computer memory requirements acceptable, a resolution of 500 μm was chosen for the revoxelization of the NURBS/PM model.

2.2 *High Resolution Model of the Lung*

To construct the high resolution model of a lung, a lung specimen[28] was scanned by a GE/phoenix|x-ray cone-beam CT "v|tome|x" (Ref. 29), which features a higher resolution than standard medical CTs, but still has a large enough volume to image the lung specimen. The dataset resulting from a scan with 60-kV tube voltage at a resolution of 114 μm encompassed 3000 slices with ~12 billion pixels (22 GB). The lung was dry and fixed in a gas-filled state. Due to the large density difference between gas and tissue, a good distinction between the tissue, the interior of the airways, and alveoles could be achieved. This procedure presented several challenges: due to technical restrictions of the imaging device, the specimen had to be scanned in three distinct operations and the resulting image datasets were then reassembled together. The volume of the CT data was reduced from 22 to 6.6 GB by removing redundant slices and the surrounding air. The model of the whole lung consists of ca. 4.5 billion voxels of $(0.11\ \mathrm{mm})^3$ dimension. Figure 4 shows a photograph of the (a) lung specimen and (b) a planar radiograph of the high resolution lung.

In order to perform imaging simulation, tissue composition and density had to be assigned to the gray values of the CT scan. For this purpose, these values have first to be related to the absorption coefficient or hounsfield units (HU). To obtain reference HU values, the lung was rescanned in a standard medical CT (GE Brightspeed 16; Ref. 30) at 80-kV tube voltage to obtain a histogram of pixel values in HU. The scanning resolution was $0.4 \times 0.4 \times 0.625\ \mathrm{mm}^3$, which was the highest obtainable resolution for this device. By comparing the histogram of pixel values in HU obtained in this scan with those of the uncalibrated gray values, a suitable transformation from gray to HU values was sought. However, since the x-ray absorption of the lung model should be close to the lung of a patient, and the lung specimen was dried—in contrast to a living person—the HU distribution of a real patient's lung was also required. Hence, the CT scan of the patient whose image data were utilized to construct the model Laura has been used for this purpose. The maximum of the resulting histogram indicated higher HU than those of the lung specimen, i.e., the average x-ray absorption of a living lung would be higher than that of the lung specimen. To account for this in the simulation, the transformation of the uncalibrated gray values was further adjusted, such that the maximum of the transformed histogram exhibits a value close to the maximum of the histogram of Laura's lung.

Finally, the resulting HU values were binned into 27 different intervals. These were then assigned to either lung parenchyma ($\mathrm{HU} < 0$), cartilage ($0 < \mathrm{HU} < 1200$), or mineral bone as a substitute for calcifications ($1200 < \mathrm{HU} < 3000$). The elemental compositions for the above tissues were taken from ICRP Publication 89.[22] The densities were adjusted to reproduce the HU values in each bin for a CT x-ray spectrum at 80 kV, which was the voltage used in the standard-resolution imaging of the lung specimen.

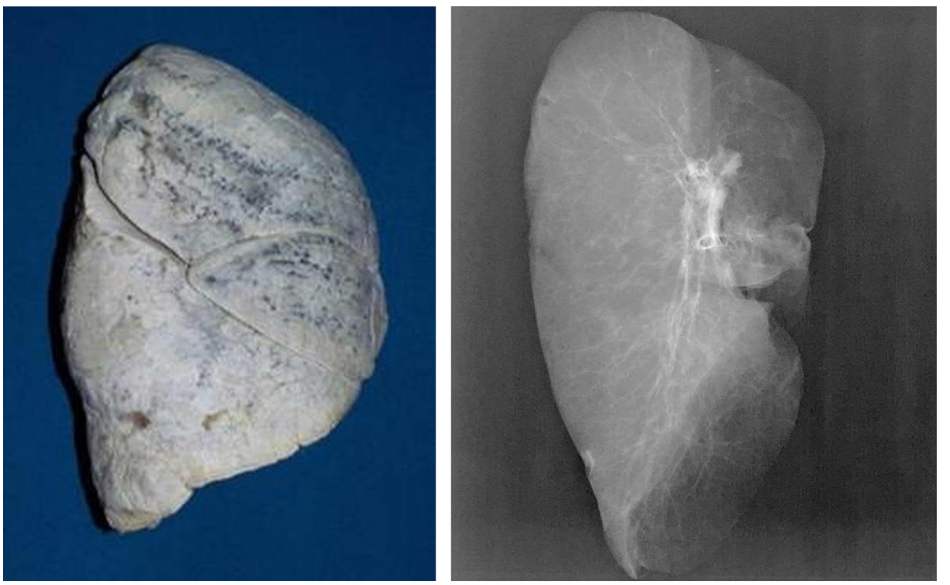

Fig. 4 (a) Photograph of the lung specimen and (b) planar radiograph of the specimen showing the bronchial fine structures and some microcalcifications.

2.3 *Image Simulations with Monte Carlo Methods*

The high resolution model of the lung has been inserted into the phantom Laura, as would be described below, and dual-lattice geometry is achieved. The particle transport inside the phantoms has been simulated with the Monte Carlo code EGSnrc[31] in version V4-2-3-0. Due to the combination of high and low resolution organs, the user code has been designed such as to be able to perform dual lattice transport by switching between two different voxel resolutions. The models consist of a three-dimensional voxel matrix, wherein each voxel is assigned a unique medium. The following media have been considered with elemental compositions according to ICRP Publication 89:[22] adipose tissue, lung, liver, muscle tissue (tissue taken for heart) and for the original Laura model, stomach-wall. The proportions of mineral bone and active and inactive bone marrow in Laura were determined for each bone voxel based on the original CT gray value, as described by Zankl and Wittmann.[32] The elemental compositions correspond to those of the ICRP reference adult female model.[4] For media assigned to the high resolution lung specimen, see Sec. 3.2.

The Monte Carlo code follows a particle through the body until it hits the image detector. Transmission, absorption, and scattering of the photons through the virtual phantom were simulated using the photon cross-sections, which agree with those of the XCOM database.[33] Photons and electrons, whose energies dropped below 10 and 100 keV, respectively, were discarded. In this way, projection images can be modeled and tissue doses can be calculated.

In order to verify the visibility of fine lung structures within the quantized noise from the low resolution surrounding anatomy, a thorax posterior examination was simulated and the projection images were modeled. First, a test calculation was performed where, for simplicity, only a portion of the entire high resolution lung model has been used and embedded in the voxel model Laura. The tube voltage was 75 kV and the filtration was 2 mm aluminum. The spectrum has been generated with the IPEM78 program by Cranley et al.[34] The focus-to-detector distance was 75 cm and the detector was 15 cm in front of the model. The detector was composed of 900×800 pixels with a pixel size of 500×500 μm^2. In the simulation, 24 billion photons were followed.

For the second test calculation, the same portion of the high resolution lung was embedded in the voxelized NURBS/PM model and the thorax posterior examination, as described above, was simulated within the hybrid/dual-lattice model.

For a further, more realistic simulation, the entire lung model was embedded in the NURBS/PM model of Laura, substituting the larger part of its left lung. The lung model, stemming from a lung specimen, is somewhat distorted compared to the lung of a living person. For this work, no attempt was made to remove this distortion. The lung model has been rotated by 25 deg around the craniocaudal axis, and the voxel dimensions have been reduced to $0.1030 \times 0.07430 \times 0.1032$ mm^3 to better fit into Laura. For the rotation, the IDL-routine "ROT" (Exelis Visual Information Solutions, Inc., Boulder, United States) has been applied using cubic convolution interpolation with an interpolation parameter of -0.5.[35] Beyond these simple rotation and scaling operations, no additional deformation has been performed. Furthermore, it was not necessary to further smooth the boundary between the inserted high resolution lung and Laura's original lung since the high resolution lung model is already smooth. The tube voltage was taken to be 110 kV and filtration was 2.5 mm Al, typical values for thorax radiographs. The focus-to-detector distance was now 115 cm, and the detector was $\approx$10 cm in front of the model. The detector had 1000×1800 pixels with a pixel size of 144×144 μm^2. For this simulation, 200 billion photons were followed, which led to a dose area product of about 1 mGy cm^2.

For comparison purposes, and for all cases stated above, simulations were also performed for the high resolution model of the lung standing on its own, i.e., not embedded in the whole phantom. To achieve similar numbers of detected photons as

in the simulations before, the numbers of histories have been reduced to 4 and 16 billion, respectively.

3 Results

3.1 *NURBS/PM Representation of the Phantom Laura*

A hybrid model based on NURBS and PM surfaces was created from the voxel model Laura. Figure 5 shows rendered images of the (a) adipose tissue and (b) skeleton, lungs, heart, liver, and stomach. These images demonstrate the anatomical precision of the hybrid model. For utilization with the Monte Carlo code EGS4nrc, a revoxelization has taken place and a resolution of 500 μm has been chosen, much finer than the resolution of the initial phantom.

In order to investigate the geometric similarity of the voxel model Laura and its NURBS/PM version, the Dice similarity coefficient (DSC) and center of mass (CoM) were evaluated for each organ. The former were computed in a coordinate system where the respective CoMs for each organ are at the origin. The DSC value is a simple and useful summary measure of spatial overlap.[36] The good agreement in the organ morphology and position is demonstrated in Tables 1 and 2, where the DSC and the distance of CoMs of some organs of Laura and its NURBS/PM counterpart are shown. The DSC was found for all organs to be 0.89 or higher and the CoM distances agree within 1 mm.

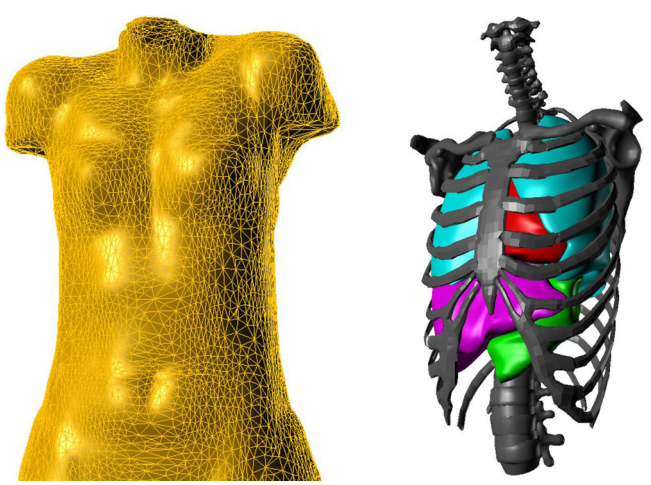

Fig. 5 (a) Adipose tissue as PM surface and (b) lungs, stomach, heart, liver as NURBS surface together with the skeleton as PM surface.

Table 1 DSC of the voxel model Laura and its NURBS/PM-based version.

Organ	DSC
Heart	0.96
Left lung	0.91
Right lung	0.93
Liver	0.93
Stomach	0.89

Table 2 Distances of COM of the voxel model Laura and its NURBS/PM-based version.

Organs	Laura	NURBS/PM-based version
Heart-left lung	6.1	6.1
Heart-right lung	10.0	9.9
Heart-liver	11.7	11.8
Heart-stomach	11.0	10.9
Left lung-right lung	12.6	12.5
Left lung-liver	16.9	16.9
Left lung-stomach	14.8	14.8
Right lung-liver	12.0	12.0
Right lung-stomach	18.4	18.3
Liver-stomach	10.8	10.9

3.2 *Voxel Media Assignment of the High-Resolution Lung Model*

The result of the calibration procedure for the gray values is shown in Fig. 6. The shape of the HU-value distribution resembles that of the standard-resolution scan of the lung specimen, scanned in a standard medical CT (see Sec. 2.2). The HU-value distribution of the perfused lung (Laura) could not be completely reproduced, particularly for the HU values larger than −700. This might have been caused by the drying process of the lung specimen, which could have led to shrinkage and thus higher density of small structures, the missing blood in the lung specimen, or by partial volume effects of the standard resolution patient CT dataset. This effect will be investigated more thoroughly in the future by using patient CT datasets of higher resolution. For the purpose of this study, i.e., to demonstrate the feasibility of the dual-lattice model for imaging optimization, the fitting is considered to be acceptable.

Figure 7 shows an example of this procedure for a single slice: in Fig. 7(a), the CT image of the high resolution scan is presented, whereas Fig. 7(b) shows the respective slice of the standard scan.

As a cross-check for the diverse gray value scaling and assignment to a medium, the mass of the lung model was determined using the original voxel dimensions of $(0.11\ \text{mm})^3$ and the respective voxel densities of Table 3: the mass of the lung model was evaluated to be about 540 g, which is about 20% heavier than the left lung mass of the reference adult female (i.e., 436 g),[22] but only about 10% heavier than the left lung of Laura with its 500 g. Thus, it can be concluded that the composition of the high resolution lung model provides a realistic representation of the composition of the human lung.

After the HU values are defined, they have to be assigned to media. In Table 3, the resulting mapping is summarized.

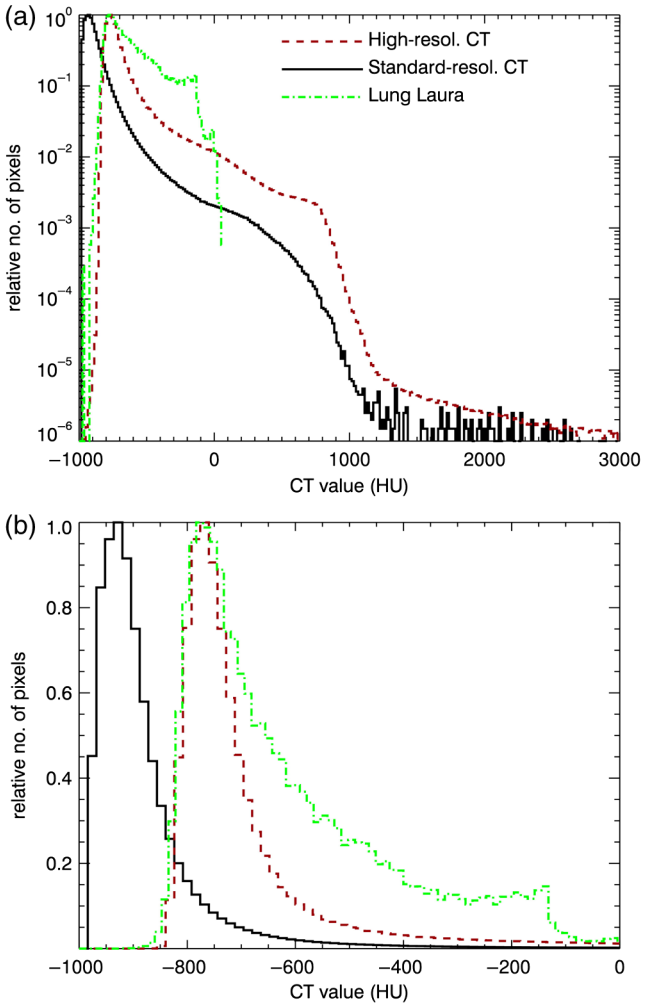

Fig. 6 (a) CT-value histogram of the standard-resolution scan of the lung specimen (black) and the lung of the patient corresponding to the model Laura (green). The red histogram represents the fit of the gray values of the high-resolution lung to both histograms, as described in Sec. 2.2. (b) Detail from (a) showing the relative pixel counts for CT values up to 0 in a linear scale.

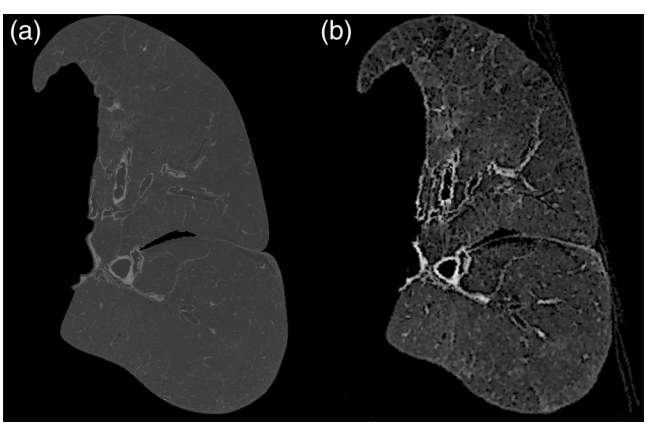

Fig. 7 (a) CT slice of the (dry) lung specimen with the high resolution scanner and (b) obtained with the clinical scanner in standard resolution.

3.3 *Test Simulations*

The high-resolution model of the lung was first fitted into the original version of the model Laura, where the original resolution (see Sec 2.1) of Laura was retained. As explained above, for the initial simulation test, for simplicity, only a portion of the entire lung model has been used and fitted on the right lung of Laura. Figure 8 (left) shows a transverse slice of the voxel model with the embedded high-resolution lung. For this test simulation, no perfect fit of the high resolution lung into Laura was attempted, and it can be seen that the original lung still covers a small portion of the thorax (shown in green). Also, as expected, the internal structures of the bones obtained from the CT image of Laura are clearly visible on the CT slice. Figure 8(a) shows the simulated image for a posterior–anterior

Table 3 Mapping of the HU values to media and their densities. The media elemental compositions are taken from ICRP Publication 89.[22]

No.	Medium	HU bins		Density (g/cm^3)
1	Air	−1000	−920.0	1.29E − 03
2	Lung	−920.0	−820.0	0.15
3		−820.0	−760.0	0.21
4		−760.0	−700.0	0.27
5		−700.0	−640.0	0.33
6		−640.0	−580.0	0.39
7		−580.0	−510.7	0.45
8		−510.7	−432.1	0.53
9		−432.1	−353.6	0.61
10		−353.6	−275.0	0.69
11		−275.0	−196.4	0.77
12		−196.4	−117.9	0.85
13		−117.9	−39.3	0.92
14		−39.3	62.5	1.00
15	Cartilage	62.5	187.5	1.12
16		187.5	312.5	1.24
17		312.5	437.5	1.37
18		437.5	562.5	1.49
19		562.5	687.5	1.62
20		687.5	812.5	1.74
21		812.5	937.5	1.86
22		937.5	1200	1.99
23	Mineral bone	1200	1600	1.88
24		1600	2000	2.20
25		2000	2400	2.51
26		2400	2800	2.82
27		2800	3200	3.14

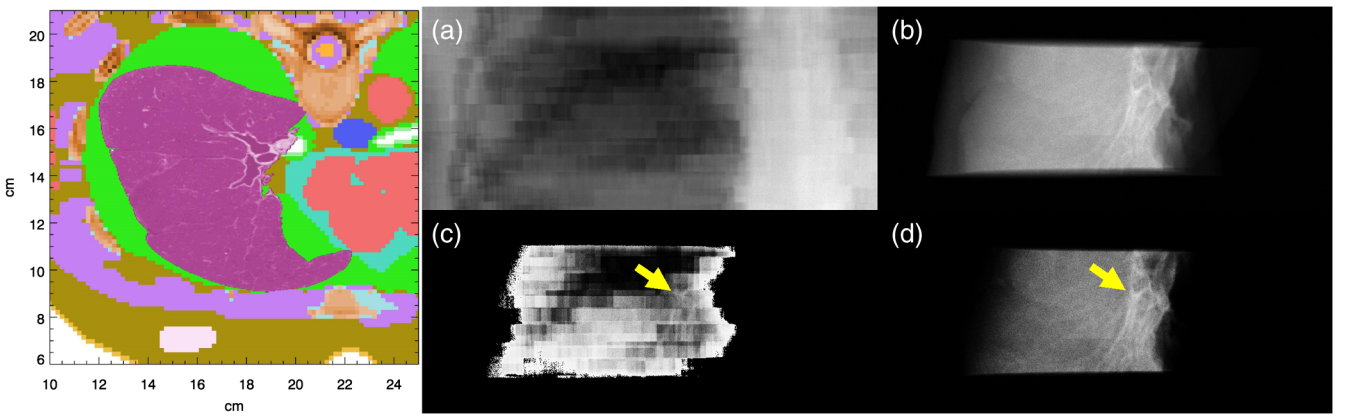

Fig. 8 Transverse slice of the voxel model with embedded high-resolution lung (left); (a) and (c) simulated posterior–anterior lung examination with the high-resolution partial model of the lung; (b) and (d) simulated posterior–anterior examination of the lung without the body model. In the lower row, the gray values are windowed specifically to make the fine structures visible, where in (c), the brightest pixels have been omitted for a better perceptibility. The yellow arrows mark an exemplary structure visible in both images. It can be seen that the voxels having low resolution appear as large steps and prohibit a clear distinction of the fine structures.

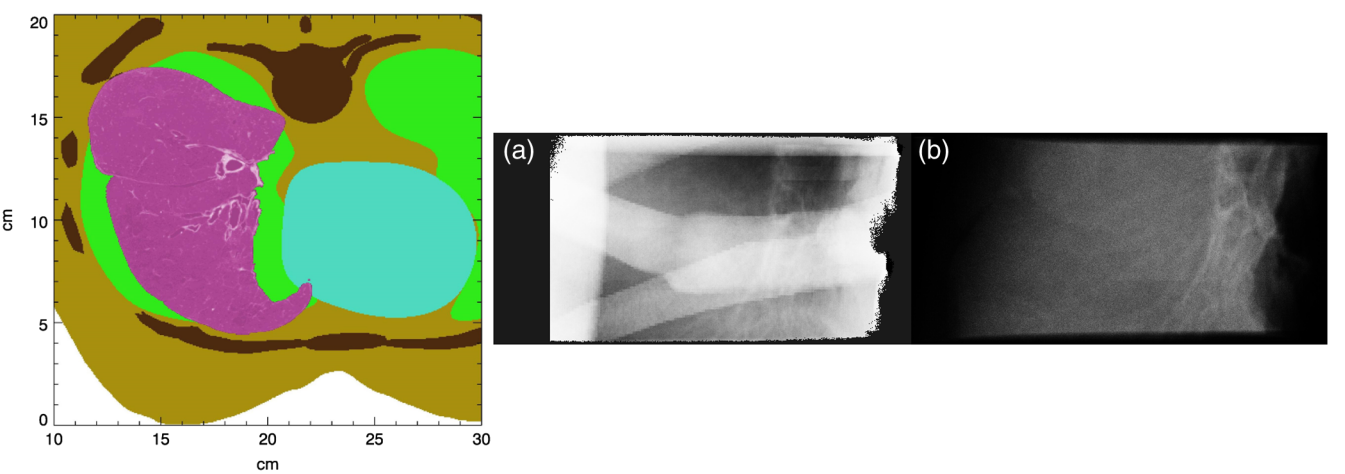

Fig. 9 Transverse slice of the "smoothed," voxel model with embedded high-resolution lung (left); simulated posterior–anterior lung examination with a high-resolution partial model of (a) the lung in the smoothed via NURBS/PM body model and (b) simulated examination of the lung without body model.

thorax radiograph with 75-kV tube voltage. For comparison purposes and for verifying whether the lung structures are visible, a simulation was performed for the lung placed on its own, i.e., outside the rest of the body; Fig. 8(b) shows the image of this simulation. Figures 8(c) and 8(d) show the same simulated images as in Figs. 8(a) and 8(b), respectively, but the gray values are windowed specifically to make the fine structures visible. It can be seen from Fig. 8(c) that the low resolution of the original Laura model results in jagged step structures, particularly at the edges of the ribs in the simulated x-ray image. These steps cover the fine structures, present in the high-resolution lung model alone, which are visible in Fig. 8(d), preventing their recognition.

For this reason, it is necessary to smooth the edges of the organs in the body model surrounding the high-resolution organ model. This was achieved by creating a NURBS/PM-based representation of the body model, as described in Sec. 2.1. Similarly, for the same irradiation conditions as for Fig. 8, the left panel of Fig. 9 shows a slice of the NURBS/PM model combined with the high-resolution lung model, at a corresponding craniocaudal height, as in Fig. 8. As described in Sec 2.1, the NURBS/PM model contains neither substructures of the heart and lungs nor organs that are not of interest for the purpose of this work, i.e., oesophagus, muscle, bronchi. Since a different, extrinsic skeleton has been taken for the NURBS/PM model, the bones (see Fig. 9) show no internal structures, as the bones shown in Fig. 8, but have smoother and slightly different outlines. In the right panel of Fig. 9, simulated images (a) of the combined model and (b) of the bare high resolution lung are shown with similar gray value windowing. It can be seen that the spine and ribs are now clearly visible and the fine structure of the lung is easily recognizable.

3.4 *Simulations of a Typical Lung Radiograph*

Figure 10(a) shows the simulation of the image when the complete model of the lung specimen is embedded in the NURBS/PM based body model for a tube voltage of 110 kV. On average, about 5000 photons were detected in each detector element within the area marked by the black box. The fine structures

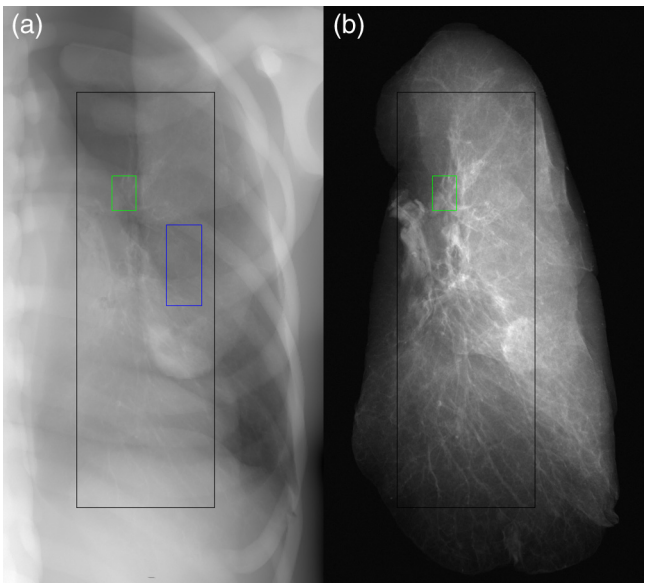

Fig. 10 (a) Simulation of a posterior–anterior lung examination with embedded high-resolution lung in the NURBS/PM based body model; (b) for comparison, the lung without the body model is shown. The gray scale is adjusted to show the full contrast range on the region of interest (black box). The regions marked by the smaller box in green and blue mark the areas magnified in Figs. 11 and 12.

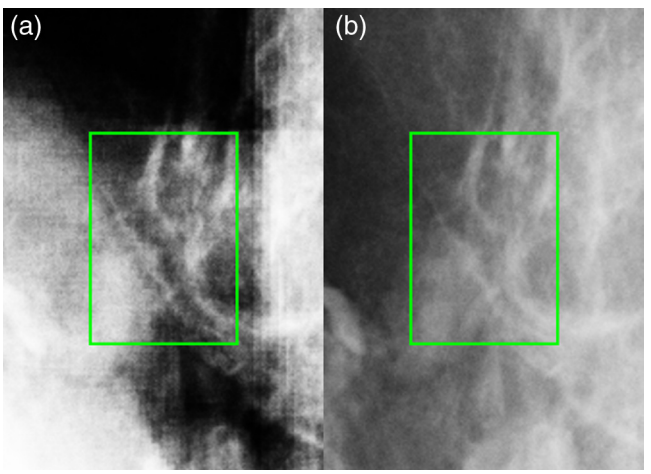

Fig. 11 Enlarged region of Fig. 10 showing fine structures of the high-resolution lung model: (a) embedded in NURBS/PM-based body model and (b) solely lung.

of the lung specimen [Fig. 10(b)] are recognizable in almost the whole image. This becomes more apparent when only small areas are considered and the gray values are windowed appropriately. As an example, in Fig. 11, a small region near the center of the image of Fig. 10 is enlarged and the gray values are adjusted. It can be seen that all details visible in the green box of Fig. 11(b) corresponding to the bare lung can also be detected in Fig. 11(a).

Figure 12 shows the image of the lung for tube voltages of (a) 110 kV and (b) 70 kV, whereas all other exposure parameters are the same. It can be seen that more structures are visible for the 110-kV tube voltage.

Thus, the influence of various technical examination parameters on the resulting image quality measures, e.g., contrast-to-noise ratio, modulation transfer function (MTF), or noise power spectrum (NPS) can be investigated with this hybrid/dual-lattice model.

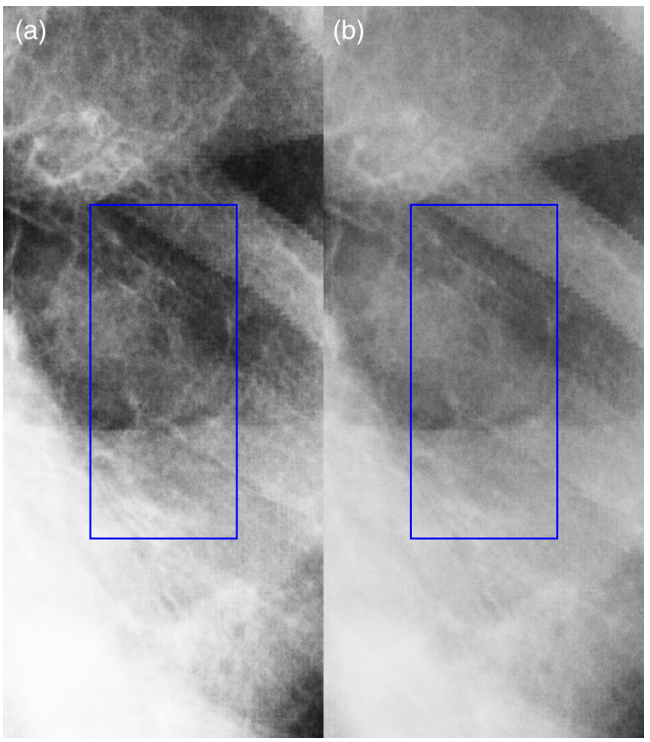

Fig. 12 Simulated image of the high-resolution lung model embedded in the NURBS/PM-based body model for (a) 110 kV and (b) 70 kV.

It can be seen, however, that the lower voxel resolution of Laura compared to the lung model is still visible as small steps at the edge of strongly absorbing structures like the projection of the ribs (e.g., Fig. 12) or as quantization artifacts when using a very narrow gray-value window, as in Fig. 11. Thus, it remains to be verified whether image-quality parameters could be determined reliably with these artifacts, or whether a higher resolution for the complete model would also be required.

4 Conclusion

Computational phantoms or models have been used up to now mostly for numerical dosimetry for the simulation of radiation inside the human body. Since the main purpose of existing models is the computation of organ/tissue doses for ionizing radiation or electromagnetic fields, their resolution is generally in the order of a few mm and cannot provide the required organ fine structures necessary for simulating realistic images and assessing image quality. Whole-body high-resolution human models can hardly be obtained due to radiation dose constraints and dual lattice voxel models, i.e., combined high and lower resolution voxel models, could be a good alternative computational tool. The purpose of this work was to examine the feasibility of dual lattice models for simulation of imaging process using a Monte Carlo code and to establish a method for determining the dependence of image quality (and dose) on imaging settings (e.g., filtration, tube voltage, etc.) for various imaging technologies.

A high-resolution voxel model of a lung has been developed by CT scans of a lung specimen (i.e., slice thickness: 114 μm, 3000 slices). Furthermore, a hybrid model based on NURBS and PM surfaces was created from a whole body voxel model, as well as its voxelized version. This type of model, compared to

conventional voxel models, presents a great improvement due to its smoothed surfaces and contours, higher resolution, and ability to modify anatomical attributes and posture. The similarity of the original voxel model and its NURBS/PM-based counterpart was found to be satisfactory.

One lobe of the lung of the hybrid model has been substituted by the high-resolution voxel lung model, resulting in a dual-lattice geometry model. It was shown that voxel models of different voxel resolutions can be combined—higher resolution in partial body (for example, lung or breast) and lower resolution in the rest of the body. However, organs surrounding the high-resolution model have to be smooth, therefore, the NURBS/PM technology for this scope is essential.

An image simulation for a lung posterior-anterior examination was performed. The lung could be clearly seen in the simulated image, together with its finer structures. Thus, the basis to investigate the influence of patient stature and technical examination parameters, such as tube voltage, filtration, and focus-to-detector distance, on various image quality measures (e.g., contrast-to-noise ratio, MTF, or NPS) by simulations has been established.

Disclosures

No conflicts of interest, financial or otherwise, are declared by the authors.

Acknowledgments

This work has been financially supported by the German Federal Ministry for the Environment, Nature Conservation and Nuclear Safety under Contract No. 3609S40002.

References

1. W. Bolch et al., "Hybrid computational phantoms for medical dose reconstruction," *Radiat. Environ. Biophys.* **49**(2), 155–168 (2010).
2. K. E. Eckerman et al., "Stylized computational phantoms developed at ORNL and elsewhere," in *Handbook of Anatomical Models for Radiation Dosimetry*, X. G. Xu and K. F. Eckerman, Eds., pp. 43–64, Taylor and Francis, Boca Raton, London, New York (2010).
3. M. Zankl, "The GSF voxel computational phantom family," in *Handbook of Anatomical Models For Radiation Dosimetry*, X. G. Xu and K. F. Eckerman, Eds., pp. 65–85, Taylor and Francis, Boca Raton, London, New York (2010).
4. ICRP, "Adult reference computational phantoms," in *ICRP Publication 110*, Elsevier, Ed., International Commission on Radiological Protection, Oxford, United Kingdom (2009).
5. Z. Habib and X. G. Xu, "Computational anthropomorphic models of the human anatomy: the path to realistic Monte Carlo modeling in radiological sciences," *Annu. Rev. Biomed. Eng.* **9**, 471–500 (2007).
6. C. Lee et al., "NURBS-based 3-D anthropomorphic computational phantoms for radiation dosimetry applications," *Radiat. Prot. Dosim.* **127**(1–4), 227–232 (2007).
7. C. Lee et al., "The UF family of reference hybrid phantoms for computational radiation dosimetry," *Phys. Med. Biol.* **55**(2), 339–363 (2010)
8. C. H. Kim et al., "A polygon-surface reference Korean male phantom (PSRK-Man) and its direct implementation in Geant4 Monte Carlo simulation," *Phys. Med. Biol.* **56**(10), 3137–3161 (2011).
9. W. P. Segars et al., "Population of anatomically variable 4D XCAT adult phantoms for imaging research and optimization," *Med. Phys.* **40**(4), 043701 (2013).
10. H. Zhong, J. Kim, and I. J. Chetty, "Analysis of deformable image registration accuracy using computational modeling," *Med. Phys.* **37**(3), 970–979 (2010).
11. M. F. Becchetti et al., "Synthesized interstitial lung texture for use in anthropomorphic computational phantoms," *Proc. SPIE* **9783**, 97835Z (2016).
12. D. Jimenez-Carretero et al., "Automatic synthesis of anthropomorphic pulmonary CT phantoms," *PloS One* **11**(1), e0146060 (2016).
13. P. R. Bakic et al., "Mammogram synthesis using a 3D simulation. I. Breast tissue model and image acquisition simulation," *Med. Phys.* **29**(9), 2131–2139 (2002).
14. P. R. Bakic et al., "Mammogram synthesis using a 3D simulation. II. Evaluation of synthetic mammogram texture," *Med. Phys.* **29**(9), 2140–2151 (2002).
15. P. R. Bakic et al., "Mammogram synthesis using a three-dimensional simulation. III. Modeling and evaluation of the breast ductal network," *Med. Phys.* **30**(7), 1914–1925 (2003).
16. C. Hoeschen et al., "A high-resolution voxel phantom of the breast for dose calculations in mammography," *Radiat. Prot. Dosim.* **114**(1–3), 406–409 (2005).
17. J. M. O'Connor et al., "Generation of voxelized breast phantoms from surgical mastectomy specimens," *Med. Phys.* **40**(4), 041915 (2013).
18. C. M. Li et al., "Methodology for generating a 3D computerized breast phantom from empirical data," *Med. Phys.* **36**(7), 3122–3131 (2009).
19. W. P. Segars et al., "Population of 100 realistic, patient-based computerized breast phantoms for multi-modality imaging research," *Proc. SPIE* **9033**, 90331X (2014).
20. D. W. Erickson et al., "Population of 224 realistic human subject-based computational breast phantoms," *Med. Phys.* **43**(1), 23–32 (2016).
21. N. Petoussi-Henss et al., "Construction of anthropomorphic hybrid, dual-lattice voxel models for optimizing image quality and dose in radiography," *Proc. SPIE* **9033**, 90331W (2014).
22. ICRP, "Basic anatomical and physiological data for use in radiological protection: reference values," in *ICRP Publication 89*, Pergamon Press, Oxford, United Kingdom (2002).
23. IDL, "Exelis Visual Information Solutions, Inc., subsidiary of Harris Corporation (Exelis VIS)," http://www.harrisgeospatial.com/ProductsandSolutions/GeospatialProducts/IDL.aspx (2012).
24. W. Vugt, "Anatomy skeleton (male) 3D model," Created Crash, 2012, http://www.creativecrash.com/marketplace/3d-models/anatomy/skeletal-system/c/anatomy-skeleton-male (March 2013).
25. Y. S. Yeom et al., "Tetrahedral-mesh-based computational human phantom for fast Monte Carlo dose calculations," *Phys. Med. Biol.* **59**(12), 3173–3185 (2014).
26. A. Badal et al., "penMesh—Monte Carlo radiation transport simulation in a triangle mesh geometry," *IEEE Trans. Med. Imaging* **28**(12), 1894–1901 (2009).
27. P. Min, "3D mesh voxelizer," 2010, http://www.google.com/search?q=binvox (2013).
28. C. Hoeschen, E. Buhr, and W. Döhring, "High-spatial-resolution measurement of x-ray intensity pattern in a radiograph of the thorax," *Proc. SPIE* **3659**, 432–443 (1999).
29. General Electric Inspection Technologies, https://www.gemeasurement.com/inspection-ndt/radiography-and-computed-tomography/phoenix-vtomex-s.
30. General Electric, http://www3.gehealthcare.com/en/products/categories/goldseal_-_refurbished_systems/goldseal_computed_tomography/goldseal_brightspeed_series.
31. I. Kawrakow et al., *The EGSnrc Code System: Monte Carlo Simulation of Electron and Photon Transport*, National Research Council of Canada (NRCC), Ottawa, Canada (2009).
32. M. Zankl and A. Wittmann, "The adult male voxel model 'Golem' segmented from whole body CT patient data," *Radiat. Environ. Biophys.* **40**(2), 153–162 (2001).
33. M. J. Berger and J. H. Hubbell, *XCOM: Photon Cross Sections on a Personal Computer*, Report No. NBSIR 87-3597, National Bureau of Standards (former name of NIST), Gaithersburg, Maryland (1987).
34. K. Cranley et al., *Catalogue of Diagnostic X-Ray Spectra and Other Data*," IPEM Report No. 78, Institute of Physics and Engineering in Medicine, New York (1997).
35. S. K. Park and R. A. Schowengerdt, "Image reconstruction by parametric cubic convolution," *Comput. Vision Graphics Image Process.* **23**(3), 258–272 (1983).
36. K. H. Zou et al., "Statistical validation of image segmentation quality based on a spatial overlap index: scientific reports," *Acad. Radiol.* **11**(2), 178–189 (2004).

Nina Petoussi-Henss is an investigator at Helmholtz Zentrum München. She holds her PhD in physics from the University of Birmingham. She has been an author of about 90 publications and

has contributed to three books. The emphasis of her work is on patient dosimetry and organ dose calculations due to medical, occupational, and environmental exposures and construction of anthropomorphic computational phantoms. She is a member of the International Commission of Radiological Protection.

Helmut Schlattl holds his PhD in physics from the Technical University in Munich, Germany. He is a senior scientist at Helmholtz Zentrum München in Germany. His research interests include radiation protection of medical staff and patients and the optimization of x-ray based imaging modalities.

Janine Becker holds her PhD in engineering sciences from the Technical University in Ilmenau, Germany. She is a research associate at Helmholtz Zentrum München. Her thesis was about the description of organ contours by means of equipotential lines of source points. Her research interest has been the construction of models of the human anatomy for radiation transport calculations. Her further research will point deeper into radiation biology toward the radiation effects from ionizing radiation.

Matthias Greiter holds his PhD in physics from the Technical University in Munich, and he is currently working at the individual monitoring service of Helmholtz Zentrum München. He is a physicist working in radiation protection, since 2004. During this time, he gradually switched topics from internal dosimetry focused on zirconium biokinetics to external dosimetry and quality control in individual monitoring, with an interlude on quality control in medical imaging.

Maria Zankl holds her diploma in mathematics from the Technical University in Munich. She is a research associate at Helmholtz Zentrum München. She has coauthored approximately 250 publications. Her main professional interests are the construction of models of the human body for radiation transport calculations and the calculation of organ dose conversion coefficients. She is the main developer of the HMGU family of voxel phantoms and of the ICRP/ICRU adult reference computational phantoms.

Christoph Hoeschen holds his PhD from Otto-von-Guericke University (OvGU). He is member of the German radiation protection board and founding chair of EURAMED platform, senior member of SPIE and AE of JMI. He is professor for medical technical systems at OvGU in Magdeburg, Germany. His main interests are new diagnostic tools and their characterization, including radiation protection. He headed a research unit at Helmholtz Zentrum München dealing with medical physics and especially diagnostics.